# FORC and TFORC analysis of Electrodeposited Magnetic Shape Memory Nanowires Array

M. Varga, L. Galdun, B. Kunca, V. Vega, J. García, V.M. Prida, E.D. Barriga-Castro, C. Luna, P. Diko, K. Saksl, R. Varga


PII: S0925-8388(21)04621-1

DOI: https://doi.org/10.1016/j.jallcom.2021.163211

Reference: JALCOM163211

To appear in: *Journal of Alloys and Compounds*

Received date: 18 August 2021
Revised date: 7 December 2021
Accepted date: 8 December 2021

Please cite this article as: M. Varga, L. Galdun, B. Kunca, V. Vega, J. García, V.M. Prida, E.D. Barriga-Castro, C. Luna, P. Diko, K. Saksl and R. Varga, FORC and TFORC analysis of Electrodeposited Magnetic Shape Memory Nanowires Array, *Journal of Alloys and Compounds,* (2021) doi:https://doi.org/10.1016/j.jallcom.2021.163211

# FORC and TFORC analysis of Electrodeposited Magnetic Shape Memory Nanowires Array

Varga M.[ab], Galdun L.[b*], Kunca B.[c], Vega V.[d], García J.[d], Prida V. M.[d], Barriga-Castro E. D.[e], Luna C.[f], Diko P.[c] Saksl K.[g], Varga R.[b]

[a]Department of Condensed Matter Physics, Pavol Jozef Šafárik University in Košice, Park Angelinum 9, 041 54 Košice
[b]Centre for Progressive Materials, Technology and Innovation Park, Pavol Jozef Šafárik University in Košice, Tr. SNP 1, 040 11, Košice, Slovak Republic
[c]Institute of Experimental Physics, Slovak Academy of Sciences, Watsonova 47, 040 01 Košice, Slovak Republic
[d]Departamento de Física, Facultad de Ciencias, Universidad de Oviedo, C/ Federico Garcia Lorca nº 18, 33007, Oviedo, Asturias, Spain
[e]Centro de Investigación en Química Aplicada (CIQA), Blvd. Enrique Reyna Hermosillo No. 140, Saltillo, Coahuila, Mexico
[f]Universidad Autónoma de Nuevo León (UANL), Av. Universidad S/N, San Nicolás de los Garza, Nuevo León, Mexico
[g]Institute of Materials Research, Slovak Academy of Sciences, Watsonova 47, 040 01 Košice, Slovak Republic
***Corresponding author**: ladislav.galdun@upjs.sk

**Abstract**:
Magnetic characterization of ferromagnetic Ni-Fe-Ga shape memory nanowires using a temperature-dependent FORC analysis is shown. The hysteresis loops' shape indicates a magnetic anisotropy that is governed by the magnetostatic interaction among neighboring nanowires. FORC measurement proved that the Ni-Fe-Ga nanowires´ array is a multi-domain and highly interacting system. The FORC analysis shows a minimal coercivity distribution that points to a uniform and homogeneous nanowires´ array. The change of the vertical spread of the FORC distribution divergence at about 395 K supports the ferromagnetic shape memory behavior and the structural transformation of the presented nanowires. The previous results are also supported by a unique TFORC analysis, showing structural changes within the transformation temperature region.

**Keywords:**
Nanowires, electrodeposition, ferromagnetic shape memory effect, FORC, TFORC,

## 1. Introduction:

The fabrication and design of advanced electronics, nanosensors, and nano-actuators is strongly dependent on the research of novel multifunctional materials [1–4]. Ferromagnetic shape memory alloys (FSMA) are among the most promising materials displaying optimal functionalities for smart electronics, sensors, and actuators [5–8]. Heusler alloys include materials with a wide range of properties. They are suitable for multifunctional applications using their multicaloric, half-metallic, or ferromagnetic shape memory behavior [9–16].

Among Heusler alloys, the $Ni_2FeGa$-based chemical composition is one of the most suitable for multifunctional applications. Ferromagnetic shape memory behavior of the Ni-Fe-Ga Heusler alloy has been investigated, and it shows strain values up to 10% under cyclic mechanical loading [17]. Structural features of the $Ni_2FeGa$ Heusler alloy reveal a characteristic $L2_1$ Heusler cubic structure at room temperature, and the alloy undergoes a martensitic transformation between the $L2_1$ high-temperature phase to the low temperature martensitic phases. Martensitic transformation temperature of the Ni-Fe-Ga Heusler alloy can be tuned by changing its chemical composition [9,18]. Its multicaloric behavior encloses an elastocaloric and magnetocaloric effect, which shows a large change of the total entropy, resulting from the combination of both the structural and magnetic phase transformations [9,19,20]. Moreover, its shape memory behavior can be used together with the multicaloric effect to produce an application-ready multifunctional material [16,21]. Its limitations depend on the fabrication technique and the resulting morphology of the prepared material. Magnetocaloric cooling devices might be prepared from the bulk samples of the Ni-Fe-Ga Heusler alloy [22], while the micro- and nanowires might work as a self-driven sensor of physical properties or as a nanoactuator in the field of biomedicine and nanoelectronics [23,24].

Preparation of nanomaterials offers new possibilities for the Ni-Fe-Ga Heusler alloy sensor and actuator applications. Multicaloric Ni-Fe-Ga thin films can be used for microchip cooling or precise temperature control during biomedical experiments and hypothermic cancer treatment [25–28]. Ni-Fe-Ga Heusler alloy nanowires offer application possibilities during the production of nano-scaled sensors and actuators, as shown in [23,24]. Moreover, since the magnetic field induced shape memory effect requires no additional energy source, the sensing and actuation process could run simultaneously [29].

However, the downsizing of a well-known material inserts additional effects into the system [30–33]. In Heusler alloys, the downsizing has been studied among the martensitic transformation temperature of thin films [34]. It has been shown that the reduction of a film thickness causes the martensite start temperature ($T_{MS}$) to decrease [30,31]. Therefore, the preparation of Heusler alloy nanowires opens a gateway towards a new research area, where the differences between the bulk and the nanodimensional materials are being studied.

In order to understand the changes that take place within a multifunctional ferromagnetic material, it is necessary to determine the materials' magnetic properties, which include the measurement of the samples' magnetization or hysteresis loops. Magnetization measurements in the form of hysteresis loops, however, may provide only limited information about the coercivity distribution [35]. Therefore, it is necessary to employ additional research methods to determine the magnetic properties of a ferromagnetic material more precisely. One of the most promising methods is the First-Order Reversal Curve (FORC) measurement [36]. The FORC analysis of a magnetic material was firstly introduced by Roberts et al., who created a connection between the Preisach model and the first-order reversal curves measured from different values of the reversal magnetic field [37]. At first, the sample is magnetically saturated with a sufficient magnetic field. Then, the magnetic field is reduced to a value of the first reversal field $H_r$, and the sample is saturated again. Material analysis using the FORC method typically consists of many (>100) measured FORCs.

Therefore, FORC measurement provides information about the distribution of the coercive and interaction field of a magnetic material. Interpretation of the measured data can also be used to determine the changes that are present within the measured sample at different temperatures. During the FORC investigation of the structural transformation of CoNi alloy nanowires, the change of the structural phase from *hcp* to *fcc* was accompanied by a modification of the FORC distribution into a more symmetric shape [38]. The FORC

material analysis is especially suitable to study the magnetic properties of a system of nanowires, because an array of ferromagnetic nanowires can be properly approximated as a multi-domain material, where each single magnetic domain would be represented by a single isolated but interacting ferromagnetic nanowire in the array [36,39–42].

On the other hand, the FORC analysis can also provide limited information on the thermal hysteresis of the structural transformation. Therefore, Temperature First Order Reversal Curve (TFORC) analysis was invented to study magnetocaloric materials [43]. Using the TFORC analysis might also provide additional insight into the structural transformation of ferromagnetic shape memory materials. The TFORC analysis implies that the results might be represented as the distribution of thermal hysterons, as with the Preisach hysterons in the conventional FORC analysis [44]. Therefore, one might be able to use the TFORC analysis as a fingerprint method, although the exact mechanism is still under discussion.

Research of application-ready multifunctional materials in the nanoscale with a single-step production process is necessary to fulfill the growing need for novel devices, such as wearable electronics, biomedical sensors, or bioinspired robotics, nanodimensional drug delivery and cancer treatment. In the case of the materials that were prepared using a large-scale preparation technique, it is necessary to define their behavior mechanism. This research aims to perform a deeper characterization of ferromagnetic shape memory Ni-Fe-Ga nanowires. To achieve this, a temperature-dependent FORC and a unique TFORC analyses were performed to test their suitability for a trivial thorough characterization of a ferromagnetic sample of nanowires array.

## 2. Experimental Part:

### 2.1. Nanowires preparation:

To prepare a large amount of nanowires, template-assisted electrochemical deposition is one of the most suitable options. At first, it is necessary to optimize the deposition conditions, which could be time-consuming. After the method optimization, the resulting nanowires are prepared in minutes and their number exceeds $10^9$ nanowires per 1 $cm^2$. The electrodeposition bath used for the preparation of the Ni-Fe-Ga nanowires within this research contained: $NiSO_4$ . $6H_2O$ (100 mM), $FeSO_4$ . $7H_2O$ (30 mM), and $Ga_2(SO_4)_3$ . $18H_2O$ (15 mM). The electrodeposition bath also contained additives: $H_3BO_3$ (50 mM), $Na_3$-Citrate . $2H_2O$ (100 mM) and $(NH_4)_2SO_4$ (100 mM). The electrodeposition was carried out as a template-assisted pulsed electrochemical process, using the anodized aluminum oxide (AAO) membrane with the diameter of the nanopores of 60 nm [45]. The deposition time was adjusted to obtain nanowires of an appropriate length, which was 7.5 μm. The growing process was performed at a laboratory temperature with a deposition pulse of 12 mA for 1 s and a resting pulse of 0 mA for 2 s. The gold nanocontacts within the AAO membrane were used as a working electrode, and a Pt grid was used as a counter.

### 2.2. Materials Characterization:

The microstructure was studied in a MIRA3 TESCAN scanning electron microscope (SEM) with a field emission cathode, equipped with AzTEC Energy Dispersive Spectroscopy (EDS) analysis system. The structural characterization was performed in a transmission electron microscope (TEM) FEI-TITAN operated at 300 kV with a Gatan CCD camera. The composition of the samples was studied with an Energy dispersive spectroscopy (EDS) detector, employed within the transmission electron microscope.

During the magnetic characterization, the nanowires were studied as-prepared in the form of an array. Magnetic measurements were performed by vibrating sample magnetometry

(VSM) in a Quantum Design MPMS® SQUID VSM system. The magnetic measurements were performed with the magnetic field applied in the parallel direction with respect to the nanowires´ longitudinal axis. The hysteresis loops were measured at the temperatures of 100 and 395 K. The temperature dependence of magnetization was measured with a temperature sweep rate of 1 K.min$^{-1}$. The FORC measurements were performed at 100, 200, 300 and 395 K. In total, there were 120 FORCs measured at each temperature with the starting point for each measured FORC lying on the descending branch of the major hysteresis loop. After the positive saturation at the magnetic field of 6 kOe, the decreasing reversal fields ranged from 5.9 kOe down to the negative saturation at the magnetic field of -6 kOe with the step of 100 Oe. As a result, a grid of $M(H, H_r)$ points was specified using a smoothing factor SF = 2 [46].

The FORC distribution is defined as a mixed second derivative of the sample magnetization with the given $H_r$ and $H$ (Equation 1):

$$\rho_{FORC}(H_r, H) = -\frac{1}{2}\frac{\partial^2 M_{FORC}(H_r, H)}{\partial H . \partial H_r}, \#(1)$$

where $\rho_{FORC}(H_r, H)$ is the FORC distribution at the given magnetic field $H$ with the reversal field $H_r$ from which the individual FORC measurements started. $M_{FORC}(H_r, H)$ represents the measured magnetization at the given magnetic fields. The results are usually displayed in the field plane with the following coordinates (Equation 2):

$$H_C = \frac{(H - H_r)}{2}, \qquad H_i = \frac{(H + H_r)}{2}, \#(2)$$

where $H_c$ represents the coercive field and $H_i$ is the interaction field within the measured specimen. The results are depicted as a 2D contour plot with the $H_c$ and $H_i$ coordinates as shown in Ref. [46].

TFORC measurement consists of individual reversal curves measured within the hysteretic region of the $M(T)$ dependence. During the cooling TFORC analysis, the sample is firstly heated above the transformation temperature, followed by a magnetization

measurement during the cooling process. Then, the temperature was reversed to a temperature $T_a = T - T_r$, where $T_r$ is the reversal temperature, and the cooling $M(T)$ dependence is measured again. The temperature sweep rate was the same as with the $M(T)$ dependence (1 K.min$^{-1}$). The TFORC analysis consists of several individual measurements with equal steps of decreasing $T_r$ values. The $M_C(T, T_r)$ values measured during the cooling TFORC analysis are evaluated according to (Equation 3):

$$\rho_C(T, T_r) = -\frac{\partial^2 M_C(T, T_r)}{\partial T \partial T_r}, \#(3)$$

where $\rho_C(T, T_r)$ is the TFORC distribution of the cooling measurement. The heating measurement is evaluated similarly, but the $\rho_H(T, T_r)$ values have a positive sign. The TFORC distribution is then plotted as a function of the temperature hysteron width ($T_h$) and its central position ($T_u$) according to [44] (Equation 4):

$$T_h = \frac{|T - T_r|}{2}, \quad T_u = \frac{T + T_r}{2} \#(4)$$

The TFORC analysis was performed at the applied magnetic field of 10 kOe to ensure the magnetic saturation of the nanowires´ sample. The nanowires were first heated up to 395 K, and the decreasing reversal temperatures ranged from 390 K to 250 K with the step of 5 K.

**3. Results and Discussion:**

The electrodeposition was performed into a well-ordered nanoporous AAO membrane, shown in Figure 1a. The nanopores within the AAO membrane have a 65 ± 4 nm diameter, with the interpore distance between the nanopores centers ≈ 105 nm. The overall chemical composition of the prepared nanowires is $Ni_{55}Fe_{43}Ga_2$ (at.%), with the deviation from the $X_2YZ$ Heusler chemical composition caused probably due to the difficult determination of the AAO membrane effective deposition area. Several spots on the individual nanowires have been used for the analysis and the composition has been measured using an EDS detector that was employed within the SEM and in the subsequent TEM analysis. The average composition of the nanowires is $Ni_{55}Fe_{43}Ga_2$. It was calculated to be in the composition interval of Ni (58 ± 5 %), Fe (40 ± 5 %) and Ga (1.5 ± 0.7 %) in atomic % The nanowires show a homogeneous morphology and a length of 7.5 μm (Figure 1b). The homogeneity of the sample was studied using an EDS mapping method (Figure 2b). It shows a homogeneous distribution of the individual elements within the nanowires.

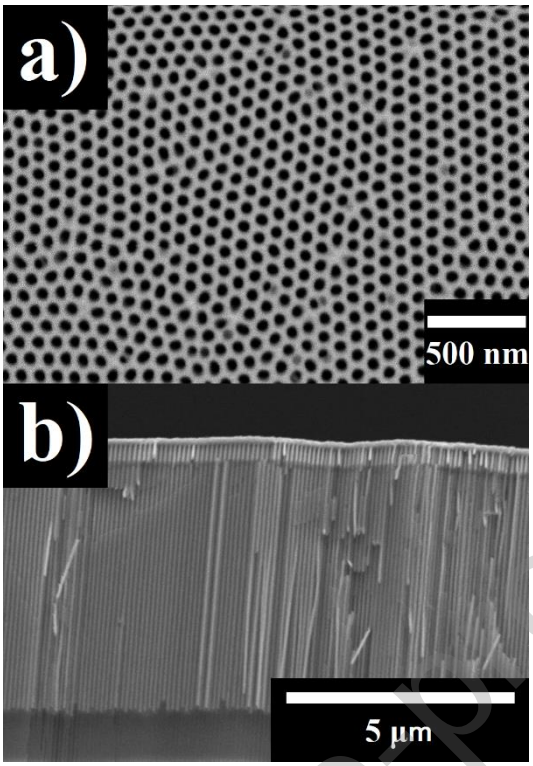


**Figure 1: a) – AAO membrane used for the nanowires preparation with a hexagonal pattern of the nanopores arrangement; b) – The prepared nanowires within the AAO membrane having the length of 7.5 µm and a homogeneous morphology**

The structural characterization of the nanowires reveals a Heusler cubic phase diffused homogeneously along the Ni-Fe rich regions of the nanowires. The structural characterization was performed using a Selective Area Electron Diffraction (SAED) method. At room temperature, it is possible to identify a Ni-Fe rich phase (a = 3.53 Å) together with a $L2_1$ cubic Heusler phase with a lattice constant $a$ = 5.745 Å and $L1_0$ tetragonal phase with the lattice parameters $a$ = 3.85 Å and $c$ = 4.31 Å (Figure 2a). The $L1_0$ tetragonal phase has been ascribed to the low-temperature martensitic state of the nanowires and the $L2_1$ Heusler phase represents the high-temperature austenite. Moreover, it is possible to observe several elongated spots within the SAED pattern (Figure 2a - red arrows), that suggest a tweed structure, which might be associated with a martensitic transformation [47]. The martensitic transformation between the L10 and L21 Heusler phases has been reported in similar temperature intervals in published research [33,48].

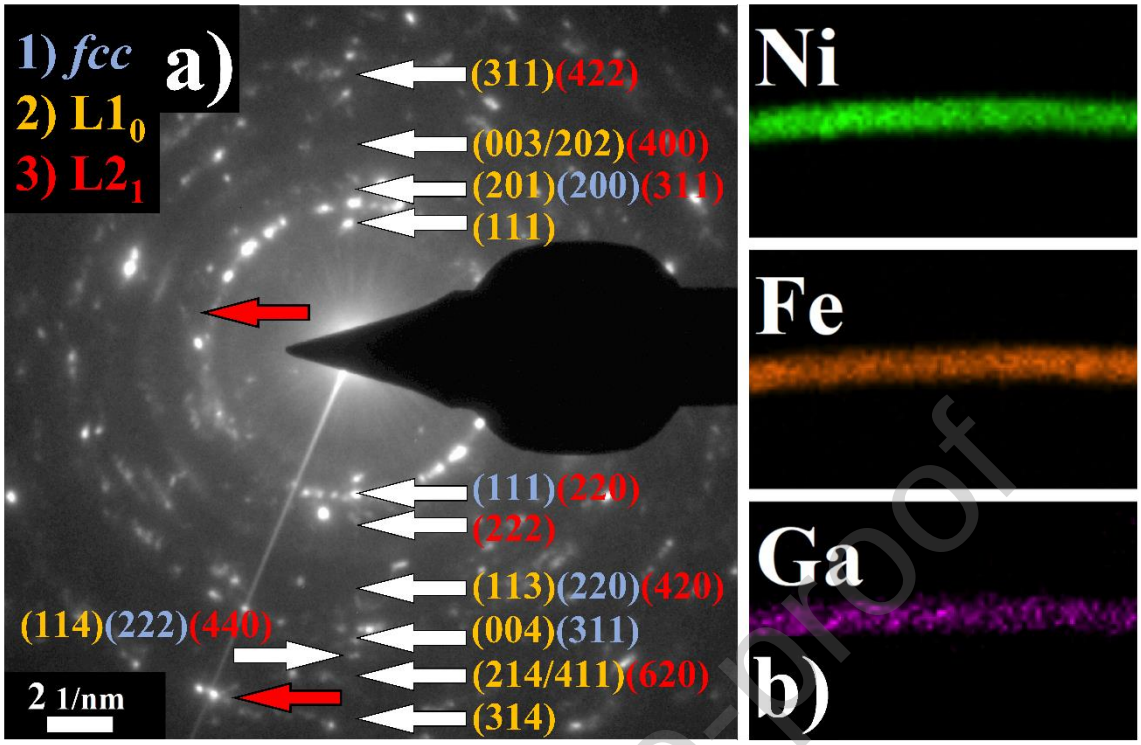


**Figure 2: a - SAED pattern of the prepared nanowires showing the corresponding Miller indices for the phases that can be identified within the nanowires. The red arrows indicate the striations, which might be caused by a martensitic transformation [49]. b - EDX maps of the individual elements within the nanowires**

Moreover, high-resolution transmission electron microscopy (HR-TEM) measurement showed a tweed contrast, that may be assigned to the ongoing structural transformation (Figure 3) [50].

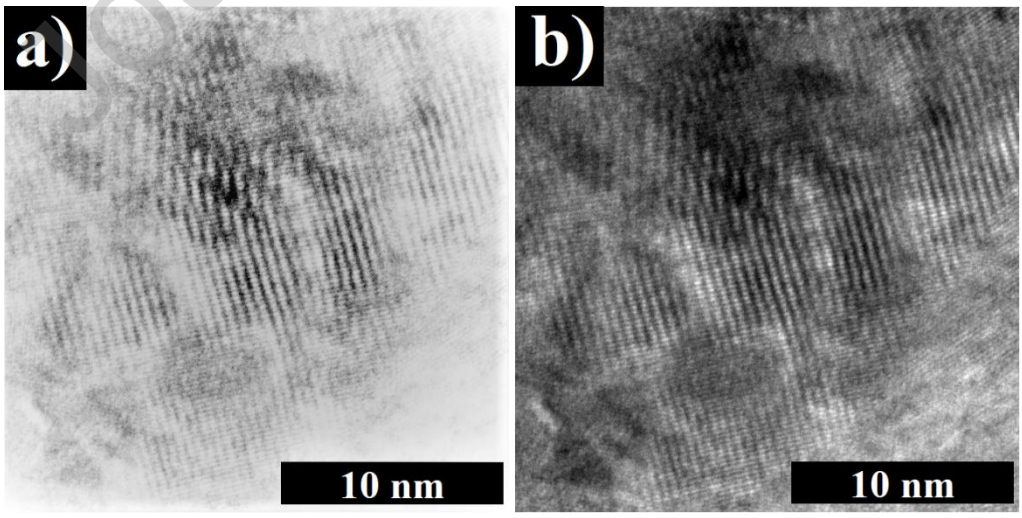


**Figure 3: Tweed contrast within the HR-TEM analysis of a single nanowire; a) false color; b) original picture**

The nanowires´ magnetization has been studied during the heating and cooling process at a low magnetic field (100 Oe) and at saturation magnetic field (10 kOe) (Figure 4). The magnetization shows a typical ferromagnetic behavior. At low magnetic field, the magnetization decreases monotonously with temperature up to 300 K where a slight increase of magnetization can be observed. Similar ferromagnetic behavior can be observed also in the cooling process, which causes an appearance of thermal hysteresis at both, low and high magnetic field measurements. The hysteresis within the magnetization – temperature ($M(T)$) dependence could be ascribed to the structural transformation between a low-temperature phase and a high-temperature austenite phase. The transformation temperatures measured from the derivative of the low magnetic field *M(T)* dependence are: Martensite start ($M_S$) = 360 K, Martensite finish ($M_F$) = 265 K, Austenite start ($A_S$) = 300 K and Austenite finish ($A_F$) = 380 K.

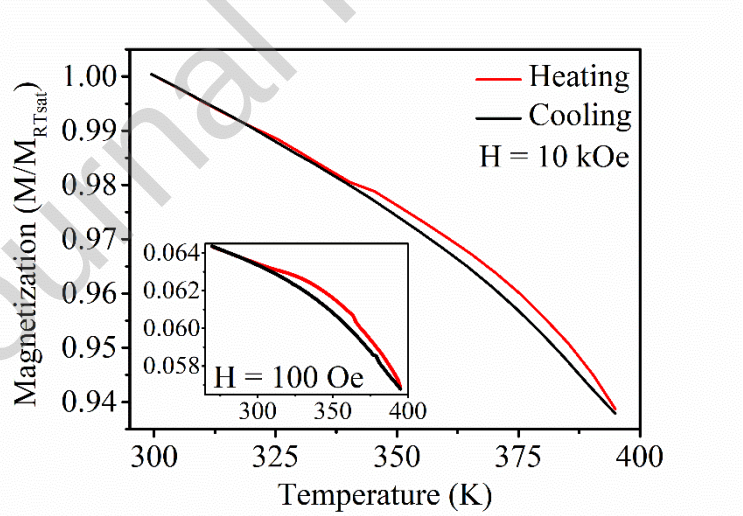


**Figure 4: High-field Magnetization-Temperature behavior normalized by the value at room temperature at 10 kOe showing a magnetization hysteresis in the temperature region from 340 K to 395 K; inset: Low-field Magnetization-Temperature dependence measured at the applied magnetic field of 100 Oe normalized to the magnetization at high magnetic field and room temperature**

Isothermal magnetization curves (Figure 5) have been measured to confirm the structural transformation at different temperatures from the magnetization hysteresis within the $M(T)$ dependence. After applying the external magnetic field at temperatures below 300 K, magnetization increases up to the magnetic field of about 6 kOe, where it slowly

approaches magnetic saturation. However, in the temperature region from 300 K to 360 K, a magnetization jump occurs within the saturation approach. The first visible magnetization jump appears during the $M(H)$ measurement at 300 K and at the magnetic field of 17 kOe. With increasing temperature, the saturation magnetic field shifts to lower values, as well as the magnetization jump, which occurs at 10 kOe and 7.5 kOe for the temperatures of 320 K and 340 K, respectively. The presented behavior may be ascribed to a ferromagnetic shape memory effect, where the structural transformation is induced by an external magnetic field [51].

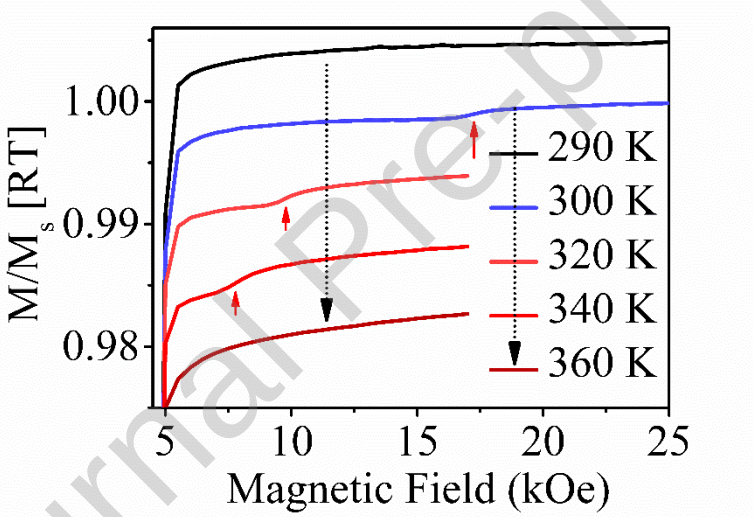


**Figure 5: Isothermal magnetization measurements normalized by the saturation magnetization value at room temperature of the Ni-Fe-Ga nanowires with the magnetization jumps being visible in the selected temperature region**

An array of magnetic nanowires can be considered as a material, where each nanowire represents an individual and at the same time identical magnetic entity or region. During the FORC and TFORC measurements, reversal curves are measured with respect to the magnetic field and temperature, respectively. In the case of magnetic nanowires array, each reversal curve represents only the nanowires that are subjected to the change of an external magnetic field or temperature. Therefore, the magnetic nanowires array may be considered as an ideal material for the FORC and TFORC analyses from its definition.

A conventional FORC analysis of the Ni-Fe-Ga nanowires was performed at four different temperatures for a deep characterization of their magnetic properties. Typical FORC measurement for the temperature of 300 K is shown in Figure 6.

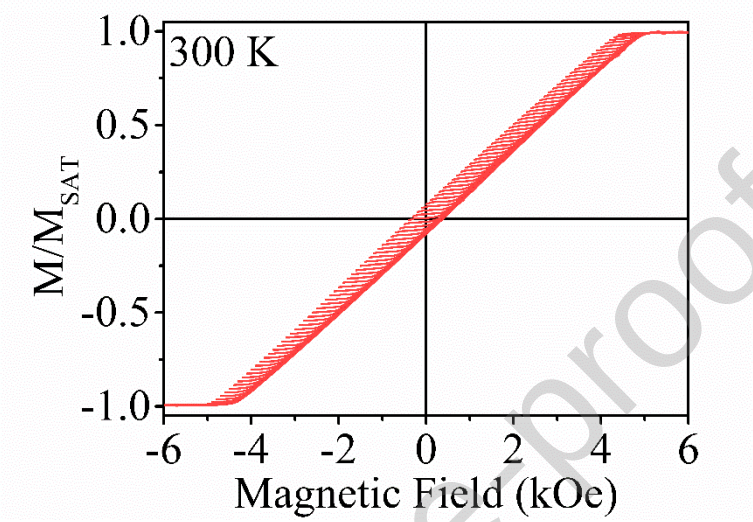


**Figure 6: Ni-Fe-Ga nanowires´ FORCs measured at the temperature of 300 K and normalized by the saturation magnetization value. The total number of the individual FORC measurements exceeds 100 for every measurement temperature.**

FORC analysis of an array of nanowires usually exhibits a two branch ("T-shape") structure [36]. One of the branches is allocated along the $H_i$ axis and intersects the $H_i = 0$ region of the FORC distribution contour plot. The second branch lies at the $H_i = 0$ axis and represents a distribution of the Preisach hysterons with a minimal interaction field but a notable coercive field distribution [36].

FORC distribution of the Ni-Fe-Ga nanowires that was calculated from the individual FORC measurements is shown in Figure 7. Contour plots of the Ni-Fe-Ga nanowires do not exhibit the usual "T-shape" structure since the branch that is parallel to the $H_c$ axis is missing. Each measurement shows a diverging FORC distribution, defined by Pike, et al. [52]. Contours within the calculated FORC distribution diagram diverge from the $H_i = 0$ axis. The FORC distribution with the diverging shape shows that the nanowires array is a multi-domain and highly interacting system, as stated by Muxworthy, et al. [53]. We can assume that the Ni-Fe-Ga nanowires exhibit a homogeneous composition within the AAO membrane, since

their $H_c$ distribution is narrow, and it does not change throughout the measurement. Nanowires´ FORC distribution also depends on the nanowires diameter and the distance between the individual nanowires. Ni-Fe-Ga nanowires show a divergence that is similar to nanowires with approximately the same diameter investigated elsewhere [54].

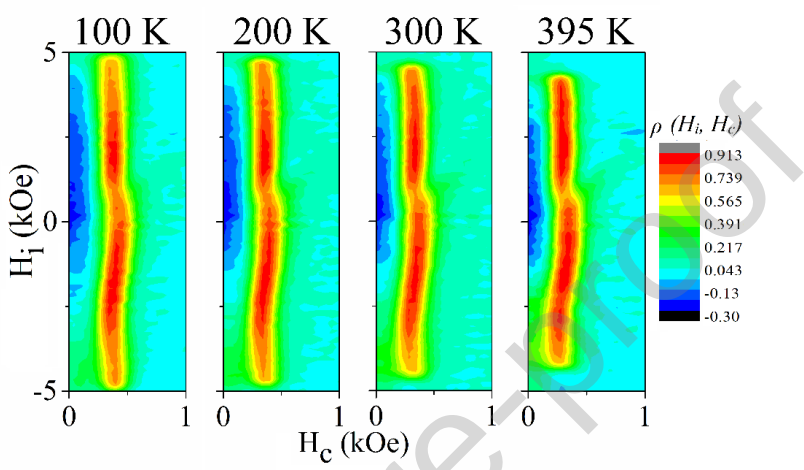


**Figure 7: FORC distribution of the Ni-Fe-Ga nanowires at different temperatures. Instead of the "T-shape" structure of the FORC distribution contour plot, the diverging FORC distribution is visible, indicating a very narrow coercivity distribution within the prepared Ni-Fe-Ga nanowires. The total spread of the FORC distribution changes significantly during the high-temperature measurement, which indicates a volume change of the Ni-Fe-Ga nanowires within the temperature range.**

The shape of the major loop within the FORC measurement (Figure 6) shows that the main contribution to the nanowires array magnetization process consists of the magnetostatic interactions of the neighboring nanowires. Similar results were shown for Heusler alloy nanowires with a different chemical composition [45]. The interaction field of the nanowires at different temperatures can be estimated as the half-width of the FORC distribution divergence ($\Delta H_i$) [54]. $\Delta H_i$ of the FORC distribution is a function of the internal demagnetization field (magnetostatic interactions within the neighboring nanowires), but it depends on several magnetic domain properties (domain cancelation, domain shape and domain wall interactions) [55]. However, the vertical spread of the diverging FORC distribution should increase with the system volume. In the case of the Ni-Fe-Ga nanowires, the diverging FORC distributions decrease with temperature. This behavior may correspond

to the contraction of the nanowires within the membrane with increasing temperature. Similar behavior was observed in the case of multi-domain magnetic nanoparticles with a strong domain wall pinning, where the diverging FORC distribution widens vertically with the nanoparticles´ increasing volume [40].

A closer inspection can be performed by extracting the coercivity variation with the measurement temperature ($\Delta H_c(T)$) from the $\rho_{FORC}$ contour plot [56,57]. For the quantitative analysis of the $\Delta H_c$ values, the $\rho_{FORC}$ coercivity dependence was extracted from the contour plot sections at different interaction fields. Then, the individual peaks were fitted with the Gaussian function. The $\Delta H_c$ values correspond to the peak´s FWHM and their values are depicted in Figure 8. It also shows the temperature dependence of the overall coercive field ($H_c$), which decreases with temperature. Such behavior is typical for ferromagnetic materials. The $\Delta H_c$ values decrease with temperature in the temperature range from 100 K to 300 K. However, the value of $\Delta H_c$ at the temperature of 395 K starts to increase. This effect may be ascribed to the magnetostructural changes within the Ni-Fe-Ga nanowires, assuming the structural transformation between the martensite phase in the low-temperature region and the cubic phase in the high-temperature region.

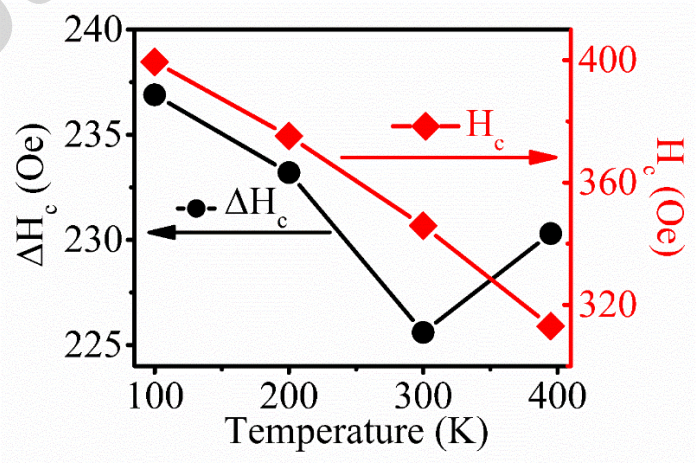


**Figure 8: $\Delta H_c$ and overall coercive field ($H_c$) values at different temperatures, showing an coercive field change difference at the temperature of 395 K**

Examination of the $\rho_{FORC}(H_r, H)$ dependence can also provide additional information about different crystallographic phases that are present within the measured sample [38]. The measurements of the $\rho_{FORC}(H_c)$ dependence at the interaction fields $H_i = 500$ Oe, $H_i = 0$ Oe and $H_i = -500$ Oe are shown in Figure 9. $\rho_{FORC}(H_c)$ at the temperatures of 100, 200 and 395 K exhibits a symmetrical Gaussian distribution (Figure 9a, b, c). However, the measurement at the temperature of 300 K shows a discrepancy between the usual Gaussian distribution and the experimental data. The $\rho_{FORC}(H_c)$ dependence at the temperature of 300 K might consist of two phases contributions since this temperature is located close to the structural transformation temperature. Therefore, the 300 K measurement was fitted with a sum of two Gaussian peaks, which provides a satisfactory resulting dependence, as shown in the right hand side of Figure 9. The individual peaks of the summary Gaussian distribution at 300 K have been ascribed to the high- and low-temperature phases according to the peak maxima of the measurements at the temperatures of 100 K and 395 K, respectively.

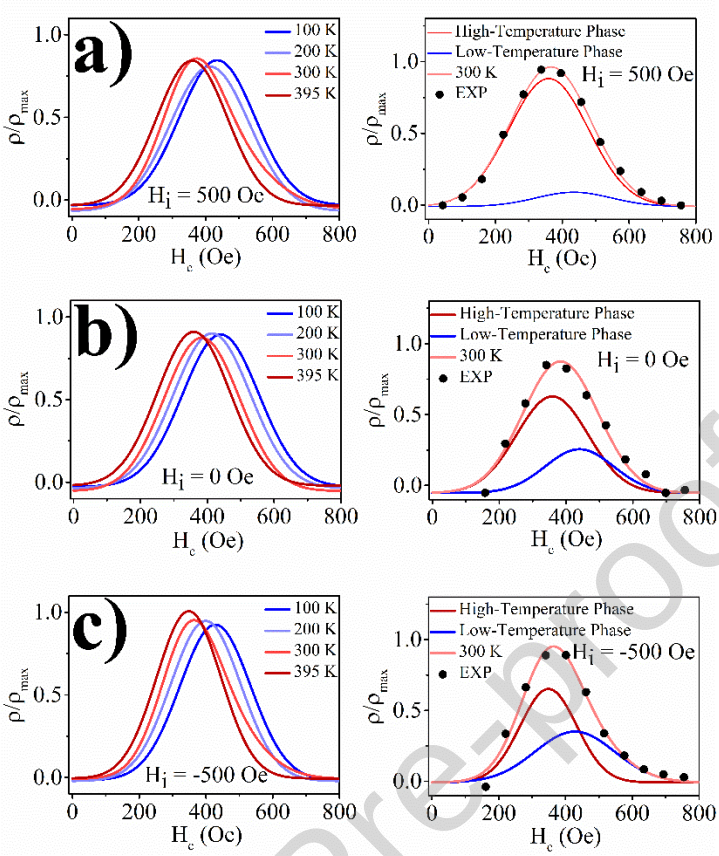


**Figure 9: Investigation of the $\rho_{FORC}$ behavior within different sections of the $\rho_{FORC}$ contour plot with respect to the interaction field (normalized by the maximal value); a), b), c) - $\rho_{FORC}$ at the interaction field of 500 Oe, 0 Oe and -500 Oe, respectively; right hand side – Gaussian distribution of $\rho_{FORC}$ represented by two phases measured at 300 K at the presented interaction fields**

Structural characterization has shown that the nanowires consist of more than one phase. Each phase has a different magnetic anisotropy and coercive field, which differs throughout the measurement. Therefore, plotting the section of the $\rho_{FORC}$ contour plot with respect to the $H_c$ axis provides further insight regarding the phases that are present within the nanowires array (Figure 10). The plots show different distributions of $\rho_{FORC}(H_c)$ with respect to the interaction field. At the coercivity value $H_c = 275$ Oe, i.e. below the coercive field of the Ni-Fe-Ga nanowires array, $\rho_{FORC}$ values exhibit two maxima, one within the negative and one in the positive interaction fields (Figure 10a). At $H_c = 335$ Oe (Figure 10b), the total coercive field of the nanowires has been exceeded at the temperature of 395 K and a change in the $\rho_{FORC}$ values is visible for the 395 K plot with a single maximum appearing around the $H_i = 0$ Oe region. At the magnetic fields applied above the total coercive field of the Ni-Fe-

Ga nanowires, a single maximum is located within the zero $H_i$ values (Figure 10c, d). In the case of the nanowires that have the coercive field of 275 Oe, the neighboring nanowires create an interaction field of $|H_i| > 1$ kOe (Figure 10a). Here, the $\rho_{FORC}$ does not change with the temperature. For the nanowires that have the coercive field of 335 Oe (Figure 10b), the $\rho_{FORC}$ behavior behaves similarly to the previous type. However, at 335 Oe the $\rho_{FORC}$ changes with temperature (Figure 10b). The change is most visible within the 395 K plot, where the neighboring nanowires belong into a different $|H_i|$ interval. Nanowires within the array that exhibit the coercive field of 395 Oe exhibit a different behavior, because their neighboring nanowires create a different interaction field at all temperatures (Figure 10c). Most of these nanowires create an interaction field $|H_i| < 2$ kOe. The remaining nanowires are subjected to the interaction field $|H_i| < 1.5$ kOe created by their neighbors (Figure 10d). Their overall coercive field is $H_c$ = 455 Oe. There was no temperature change visible within the last part of the membrane. These results imply that the nanowires membrane consists of several regions where different phases are dominant. It corresponds to the structural characterization that was performed previously on the same nanowires (Figure 2a). It shows that the nanowires consist of several phases with the dominant Ni-Fe rich phase with a homogeneously diffused Heusler phase. Only the phase within the nanowires that is capable of structural transformation is transforming. Therefore, the change of the $\rho_{FORC}$ with respect to the interaction field is not visible at every coercive field. The change within the 395 K plot at $H_c = 335\ Oe$ (Figure 10b) might represent the nanowires with the ongoing structural transformation.

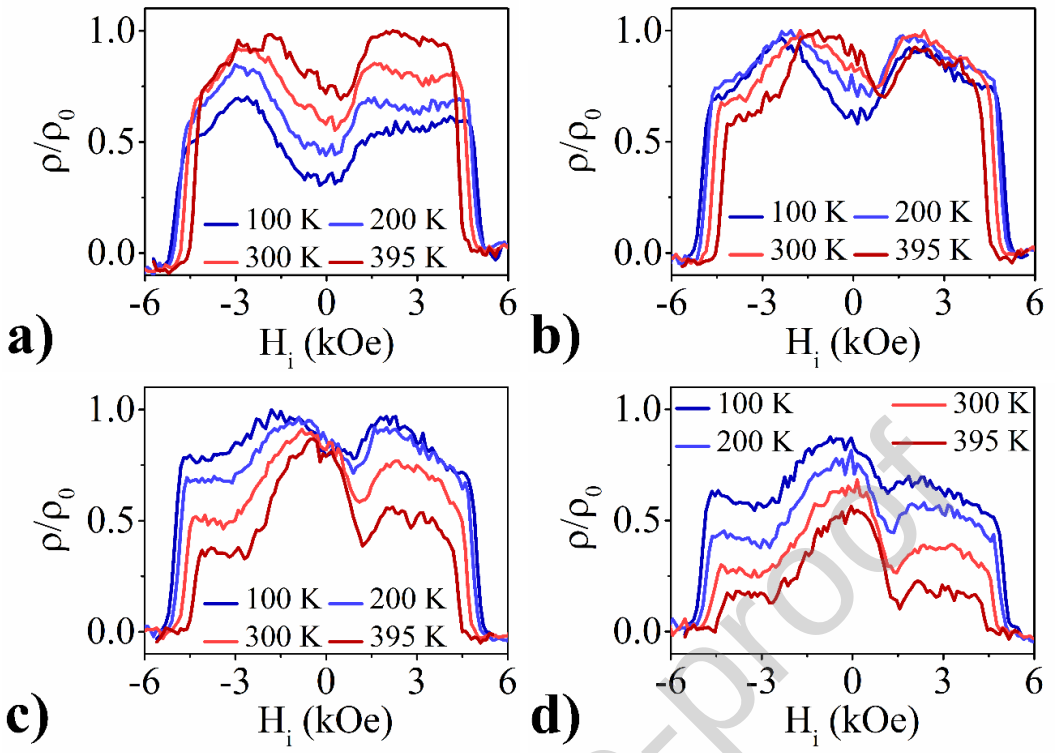


**Figure 10: $\rho_{FORC}$ dependence on interaction field measured at different coercive fields (normalized by the maximal value): a) – $H_c$ = 275 Oe; b) – $H_c$ = 335 Oe; c) – Hc = 395 Oe and d) - $H_c$ = 455 Oe**

A deeper analysis of the structural transformation was performed using the TFORC measurement technique to study the transformation temperature region. The TFORC analysis was performed following the cooling behavior of the previous measurements and the reversal temperature step was 5 K. Some of the measured TFORCs are shown in Figure 11a. At first, the magnetization increases in the temperature range from 390 to 255 K. Measurements from the reversal temperatures between 390 K and 380 K show a similar behavior. However, magnetization during the measurements from the reversal temperatures from 380 K to 320 K behaves differently. In the first stages of the measurement, the magnetization does not follow the previous behavior and returns to the original values after several temperature steps. The difference of the magnetization from the previous measurements corresponds to the magnetization hysteresis within the $M(T)$ measurement and the TFORC distribution was calculated within this region (Figure 11b). Unlike the conventional FORC measurement, the TFORC distribution is not evenly distributed within the contour plot. The difference may be

explained in terms of different approaches of FORC and TFORC analysis. While the FORC analysis includes the behavior of every magnetic phase within the studied system, the TFORC measurement is only sensitive to the phases that are capable of a phase transformation.

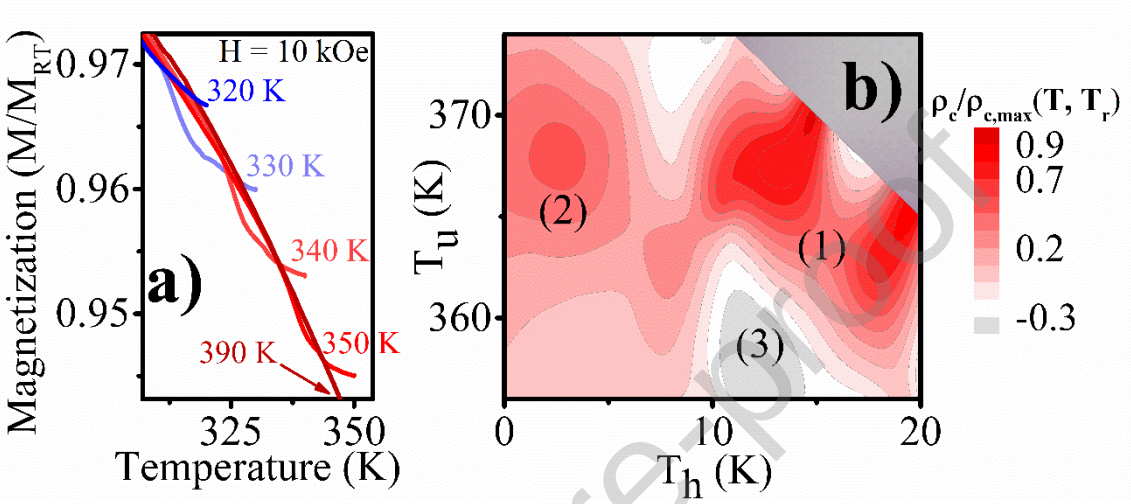


**Figure 11: a) - Measurements of the individual TFORCs showing only the plots with the temperature step of 10 K between 320 and 390 K (normalized by the maximal value); b) – TFORC distribution in the selected temperature range; Regions (1) and (2) correspond to the structural transformation of the phases present within the Ni-Fe-Ga nanowires; Region (3) represents a tail of negative values, arising probably due to the cooling behavior of the TFORCs measurement**

Figure 11b shows the TFORC distribution contour plot. The contours within the TFORC distribution are flat in the temperature range from 250 to 320 K ($T_u$ axis of the TFORC diagram). However, at the temperature of ≈ 350 K, several features begin to appear. In region (1), a sharp maximum is observed between the temperatures of 360 and 380 K. The contours visible within the (1) and (2) regions of the TFORC distribution (Figure 11b) appear in a narrow $T_u$ region, which also supports the discussion about the sample homogeneity following the FORC analysis. The sharp maxima appear in the middle of the structural transformation region derived from the $M(T)$ measurement. The sharp maximum within the TFORC distribution was ascribed to the martensitic transformation of the Ni-Fe-Ga nanowires according to the previous measurements. The transformation also appears within the region (2), which corresponds to other phases present in the nanowires. Another explanation of the multiple maxima might be found when looking into the substrate constraints. It has been

observed that the martensitic transformation was substrate-constrained during a research of a ferromagnetic shape memory Ni-Mn-Ga Heusler thin films [58].The results showed a step-like transformation behavior, which could be induced within the studied Ni-Fe-Ga nanowires by the AAO membrane. $T_u$ axis of the contour plot represents the transformation temperature region, where the temperature range is narrow, represented by sharp maxima in the region (1) and (2). Temperature hysteresis of the structural transformation can be found on the $T_h$ axis of the TFORC distribution contour plot. In region (3), the TFORC distribution values exhibit a tail with negative values, which has been previously ascribed to the nature of the measurement [43]. The overall shape of the TFORC distribution implies that the structural transformation of the individual phases is symmetric because the shape of the individual maxima is circular in nature. However, transformation rate seems to be different at various stages, because of the ridges that form throughout the measurement. The nature of the ridges was discussed within the original research regarding the TFORC measurement technique [44]. The ridges might be formed during the cooling measurement because the transformation from the austenitic to the martensitic phase is slow. The change of the transformation rate might cause an asymmetry associated with magnetization differences at high temperatures, following the discussion in the previous research on TFORC analysis of magnetocaloric materials development [43], therefore creating the ridges that appear within the measured TFORC distribution.

**4. Conclusions:**

Ni-Fe-Ga nanowires have been prepared using a template-assisted electrodeposition method. They exhibit several unusual properties, such as magnetization hysteresis during the measurement of the magnetization-temperature dependence, and magnetization jumps during the isothermal magnetization analysis, which may be attributed to a ferromagnetic shape memory behavior. A structural transformation might be represented by tweed contrast that

was present during the room temperature HR-TEM analysis. Structural analysis shows a presence of martensitic $L1_0$ and austenitic $L2_1$ phase distributed homogenously along the Ni-Fe rich region of the nanowires.

FORC analysis shows that the nanowires´ array behaves as a multi-domain and highly interacting system. The results point to the fact that the nanowires within the array exhibit a uniform chemical composition and homogeneous magnetic nature. The uniformity and homogeneity of the Ni-Fe-Ga nanowires result from the lack of the FORC distribution horizontal branch, which points to minimal coercive field distribution. Divergence along the $H_i$ axis of the FORC distribution narrows with increasing temperature and the most visible change is seen between the room temperature measurement and 395 K. This change indicates an ongoing volume change within the temperature range.

TFORC analysis shows high maxima within the temperature region corresponding to the structural transformation temperature region from the $M(T)$ dependence performed at the high magnetic field. These maxima suggest a phase transformation within the specified temperature region.

Therefore, FORC and TFORC analyses are a promising tool for the characterization of the magnetic properties of the Ni-Fe-Ga nanowires, which show a high application potential in the field of nanodimensional sensors and actuators for biomedicine or smart electrical engineering.

**CRediT authorship contribution statrment**

Michal Varga (Data curation: Lead; Investigation: Lead; Writing – original draft: Lead). Ladislav Galdun (Conceptualization: Equal; Resources: Supporting; Supervision: Lead; Writing – review & editing: Lead). Branislav Kunca (Investigation: Equal), Victor Vega (Investigation: Equal; Writing – review & editing: Equal). Javier García (Writing – review & editing: Equal). Victor M. Prida (Supervision: Equal; Writing – review & editing: Equal). Enrique Diaz Barriga-Castro (Data curation: Equal; Investigation: Equal). Carlos Luna (Data curation: Equal; Investigation: Equal; Supervision: Equal; Writing –. review & editing: Equal)Pavel Diko (Resources: Equal). Karel Saksl (Supervision: Equal). Rastislav Varga (Conceptualization: Equal; Project administration: Equal; Resources: Lead; Supervision: Equal; Validation: Equal; Writing – review & editing: Equal)

**Declaration of Competing Interest**

☒ The authors declare that they have no known competing financial interests or personal relationships that could have appeared to influence the work reported in this paper.

☐The authors declare the following financial interests/personal relationships which may be considered as potential competing interests:

**Acknowledgement:**
This work was supported by Slovak Grant Agency, APVV-17-0008, APVV-16-0079, APVV-19-0369, APVV-20-0205, APVV-20-0068, APVV-20-0138, VEGA 1/0053/19, VEGA 2/0171/19, VEGA 2/0013/19, PP-COVID-20-0025 and VVGS-PF-2020-1420. The authors also thank Universidad Autónoma de Nuevo León (Mexico) for the financial support under project PAICYT2020-CE11337-20). Spanish MCINN under research project Nº MCI-20-PID2019-108075RB-C32-MAT is also acknowledged.

**References:**

[1] J. Shi, S. Liu, L. Zhang, B. Yang, L. Shu, Y. Yang, M. Ren, Y. Wang, J. Chen, W. Chen, Y. Chai, X. Tao, Smart Textile-Integrated Microelectronic Systems for Wearable Applications, Adv. Mater. 32 (2020) 1901958. https://doi.org/10.1002/adma.201901958.
[2] M. Thomas, O. Heczko, J. Buschbeck, Y.W. Lai, J. McCord, S. Kaufmann, L. Schultz, S. Fähler, Stray-field-induced actuation of free-standing magnetic shape-memory films, Adv. Mater. 21 (2009) 3708–3711. https://doi.org/10.1002/adma.200900469.
[3] B. Wang, K. Kostarelos, B.J. Nelson, L. Zhang, Trends in Micro-/Nanorobotics: Materials Development, Actuation, Localization, and System Integration for Biomedical Applications, Adv. Mater. 33 (2021) 2002047. https://doi.org/10.1002/adma.202002047.
[4] S.A. Wilson, R.P.J. Jourdain, Q. Zhang, R.A. Dorey, C.R. Bowen, M. Willander, Q.U. Wahab, M. Willander, S.M. Al-hilli, O. Nur, E. Quandt, C. Johansson, E. Pagounis, M. Kohl, J. Matovic, B. Samel, W. van der Wijngaart, E.W.H. Jager, D. Carlsson, Z. Djinovic, M. Wegener, C. Moldovan, E. Abad, M. Wendlandt, C. Rusu, K. Persson, New materials for micro-scale sensors and actuators. An engineering review, Mater. Sci. Eng. R Reports. 56 (2007) 1–129. https://doi.org/10.1016/j.mser.2007.03.001.

[5] M. Takhsha Ghahfarokhi, F. Casoli, S. Fabbrici, L. Nasi, F. Celegato, R. Cabassi, G. Trevisi, G. Bertoni, D. Calestani, P. Tiberto, F. Albertini, Martensite-enabled magnetic flexibility: The effects of post-growth treatments in magnetic-shape-memory Heusler thin films, Acta Mater. 187 (2020) 135–145. https://doi.org/10.1016/j.actamat.2020.01.049.
[6] H.R. Zhang, G.H. Wu, Atomic-size effect on the microstructural properties of Ni2FeGa, Acta Mater. 59 (2011) 1249–1258. https://doi.org/10.1016/j.actamat.2010.10.057.
[7] W.M. Yuhasz, D.L. Schlagel, Q. Xing, K.W. Dennis, R.W. McCallum, T.A. Lograsso, Influence of annealing and phase decomposition on the magnetostructural transitions in Ni50 Mn39 Sn11, J. Appl. Phys. 105 (2009). https://doi.org/10.1063/1.3067855.
[8] Z.Y. Wei, E.K. Liu, J.H. Chen, Y. Li, G.D. Liu, H.Z. Luo, X.K. Xi, H.W. Zhang, W.H. Wang, G.H. Wu, Realization of multifunctional shape-memory ferromagnets in all- d -metal Heusler phases, Appl. Phys. Lett. 107 (2015) 022406. https://doi.org/10.1063/1.4927058.
[9] M. Hennel, L. Galdun, T. Ryba, R. Varga, Transition temperature tuning of Ni2FeGa based Heusler alloys in form of glass-coated microwires, J. Magn. Magn. Mater. 511 (2020) 166973. https://doi.org/10.1016/j.jmmm.2020.166973.
[10] R. Mahat, S. KC, D. Wines, S. Regmi, U. Karki, Z. Li, F. Ersan, J.Y. Law, C. Ataca, V. Franco, A. Gupta, P. LeClair, Influence of Cr-substitution on the structural, magnetic, electron transport, and mechanical properties of Fe3−xCrxGe Heusler alloys, J. Magn. Magn. Mater. 521 (2021) 167398. https://doi.org/10.1016/j.jmmm.2020.167398.
[11] R. Mahat, S. KC, D. Wines, F. Ersan, S. Regmi, U. Karki, R. White, C. Ataca, P. Padhan, A. Gupta, P. LeClair, Tuneable structure and magnetic properties in Fe3−xVxGe alloys, J. Alloys Compd. 830 (2020) 154403. https://doi.org/10.1016/j.jallcom.2020.154403.
[12] S. Kc, R. Mahat, S. Regmi, A. Mukherjee, P. Padhan, R. Datta, W.H. Butler, A. Gupta, P. Leclair, Tunable properties and potential half-metallicity in (Co2-xTix)FeGe Heusler alloys: An experimental and theoretical investigation, Phys. Rev. Mater. 3 (2019) 1–17. https://doi.org/10.1103/PhysRevMaterials.3.114406.
[13] E. Villa, C.O. Aguilar-Ortiz, A. Nespoli, P. Álvarez-Alonso, J.P. Camarillo-Garcia, D. Salazar, F. Passaretti, H. Flores-Zúñiga, H. Hosoda, V.A. Chernenko, Tailoring thermomechanical treatment of Ni-Fe-Ga melt-spun ribbons for elastocaloric applications, J. Mater. Res. Technol. 8 (2019) 4540–4546. https://doi.org/10.1016/j.jmrt.2019.07.067.
[14] Z.H. Liu, M. Zhang, Y.T. Cui, Y.Q. Zhou, W.H. Wang, G.H. Wu, X.X. Zhang, G. Xiao, Martensitic transformation and shape memory effect in ferromagnetic Heusler alloy Ni2FeGa, Appl. Phys. Lett. 82 (2003) 424–426. https://doi.org/10.1063/1.1534612.
[15] D.S. Kuchin, E.T. Dilmieva, Y.S. Koshkid'ko, A.P. Kamantsev, V. V. Koledov, A. V. Mashirov, V.G. Shavrov, J. Cwik, K. Rogacki, V. V. Khovaylo, Direct measurement of shape memory effect for Ni 54 Mn 21 Ga 25 , Ni 50 Mn 41.2 In 8.8 Heusler alloys in high magnetic field, J. Magn. Magn. Mater. 482 (2019) 317–322. https://doi.org/10.1016/j.jmmm.2019.02.087.
[16] M. Imrad, X. Zhang, Ferromagnetic shape memory Ni-Fe-Ga alloy foams for elastocaloric cooling, J. Phys. D. Appl. Phys. 53 (2020) 245503. https://doi.org/https://doi.org/10.1088/1361-6463/ab7df1.
[17] C. Efstathiou, H. Sehitoglu, P. Kurath, S. Foletti, P. Davoli, Fatigue response of NiFeGa single crystals, Scr. Mater. 57 (2007) 409–412. https://doi.org/10.1016/j.scriptamat.2007.04.049.

[18] Y. Li, D. Zhao, J. Liu, Giant and reversible room-temperature elastocaloric effect in a single-crystalline Ni-Fe-Ga magnetic shape memory alloy, Sci. Rep. 6 (2016) 1–11. https://doi.org/10.1038/srep25500.
[19] G.J. Pataky, E. Ertekin, H. Sehitoglu, Elastocaloric cooling potential of NiTi, Ni2FeGa, and CoNiAl, Acta Mater. 96 (2015) 420–427. https://doi.org/10.1016/j.actamat.2015.06.011.
[20] V. Franco, J.S. Blázquez, J.J. Ipus, J.Y. Law, L.M. Moreno-Ramírez, A. Conde, Magnetocaloric effect: From materials research to refrigeration devices, Prog. Mater. Sci. 93 (2018) 112–232. https://doi.org/10.1016/j.pmatsci.2017.10.005.
[21] N.M. Bruno, I. Karaman, Y.I. Chumlyakov, Orientation Dependence of the Elastocaloric Effect in Ni54Fe19Ga27 Ferromagnetic Shape Memory Alloy, Phys. Status Solidi Basic Res. 255 (2018) 1700437. https://doi.org/10.1002/pssb.201700437.
[22] D. Lewandowski, P. Płuszka, Z. Malecha, Simplified numerical model of magnetocaloric cooling device, J. Power Technol. 99 (2019) 58–66.
[23] K. Javed, X.M. Zhang, S. Parajuli, S.S. Ali, N. Ahmad, S.A. Shah, M. Irfan, J.F. Feng, X.F. Han, Magnetization behavior of NiMnGa alloy nanowires prepared by DC electrodeposition, J. Magn. Magn. Mater. 498 (2020) 166232. https://doi.org/10.1016/j.jmmm.2019.166232.
[24] J.L. Wang, M. Hassan, J.W. Liu, S.H. Yu, Nanowire Assemblies for Flexible Electronic Devices: Recent Advances and Perspectives, Adv. Mater. 30 (2018) 1803430. https://doi.org/10.1002/adma.201803430.
[25] J. Fernandes, E. Vendramini, A.M. Miranda, C. Silva, H. Dinis, V. Coizet, O. David, P.M. Mendes, Design and performance assessment of a solid-state microcooler for thermal neuromodulation, Micromachines. 9 (2018). https://doi.org/10.3390/mi9020047.
[26] R. Das, R. Prabhu, N. Venkataramani, S. Prasad, L. Li, M.H. Phan, V. Keppens, D. Mandrus, H. Srikanth, Giant low-field magnetocaloric effect and refrigerant capacity in reduced dimensionality EuTiO3 multiferroics, J. Alloys Compd. 850 (2021) 1–7. https://doi.org/10.1016/j.jallcom.2020.156819.
[27] T. Tsukamoto, M. Esashi, S. Tanaka, Magnetocaloric cooling of a thermally-isolated microstructure, J. Micromechanics Microengineering. 22 (2012). https://doi.org/10.1088/0960-1317/22/9/094008.
[28] M.A. Hamad, Magnetocaloric effect in (001)-oriented MnAs thin film, J. Supercond. Nov. Magn. 27 (2014) 263–267. https://doi.org/10.1007/s10948-013-2254-9.
[29] R.C. O'Handley, S.J. Murray, M. Marioni, H. Nembach, S.M. Allen, Phenomenology of giant magnetic-field-induced strain in ferromagnetic shape-memory materials (invited), J. Appl. Phys. 87 (2000) 4712–4717. https://doi.org/10.1063/1.373136.
[30] J. Meyer, N. Teichert, A. Auge, C. Wang, A. Hutten, C. Felser, Heusler Compounds Go Nano, in: C. Felser, A. Hirohata (Eds.), Heusler Alloy. Prop. Growth, Appl., Springer International Publishing, 2015: pp. 111–132. https://doi.org/10.1007/978-3-319-21449-8.
[31] M. Salaheldeen, V. Vega, R. Caballero-Flores, V.M. Prida, A. Fernández, Influence of nanoholes array geometrical parameters on magnetic properties of Dy-Fe antidot thin films, Nanotechnology. 30 (2020) 455703. https://doi.org/10.1088/1361-6528/ab36cc.
[32] N. Ozdemir, SIZE EFFECTS IN FERROMAGNETIC SHAPE MEMORY ALLOYS, 2012.
[33] N. Ozdemir, I. Karaman, N.A. Mara, Y.I. Chumlyakov, H.E. Karaca, Size effects in the superelastic response of Ni 54Fe 19Ga 27 shape memory alloy pillars with a two stage

martensitic transformation, Acta Mater. 60 (2012) 5670–5685. https://doi.org/10.1016/j.actamat.2012.06.035.
[34] L. Straka, J. Drahokoupil, O. Pacherová, K. Fabiánová, V. Kopecký, H. Seiner, H. Hänninen, O. Heczko, The relation between lattice parameters and very low twinning stress in Ni50Mn25+xGa25-x magnetic shape memory alloys, Smart Mater. Struct. 25 (2016) 025001. https://doi.org/10.1088/0964-1726/25/2/025001.
[35] R. Lavin, J.C. Denardin, J. Escrig, D. Altbir, A. Cortés, H. Gómez, Magnetic characterization of nanowire arrays using first order reversal curves, IEEE Trans. Magn. 44 (2008) 2808–2811. https://doi.org/10.1109/TMAG.2008.2001814.
[36] C.I. Dobrotə, A. Stancu, Tracking the individual magnetic wires' switchings in ferromagnetic nanowire arrays using the first-order reversal curves (FORC) diagram method, Phys. B Condens. Matter. 457 (2015) 280–286. https://doi.org/10.1016/j.physb.2014.10.006.
[37] A.P. Roberts, C.R. Pike, K.L. Verosub, First-order reversal curve diagrams: A new tool for characterizing the magnetic properties of natural samples, J. Geophys. Res. Solid Earth. 105 (2000) 28461–28475. https://doi.org/10.1029/2000jb900326.
[38] A.S. Samardak, A. V. Ognev, A.Y. Samardak, E. V. Stebliy, E.B. Modin, L.A. Chebotkevich, S. V. Komogortsev, A. Stancu, E. Panahi-Danaei, A. Fardi-Ilkhichy, F. Nasirpouri, Variation of magnetic anisotropy and temperature-dependent FORC probing of compositionally tuned Co-Ni alloy nanowires, J. Alloys Compd. 732 (2018) 683–693. https://doi.org/10.1016/j.jallcom.2017.10.258.
[39] J. Xu, J. Zhang, J. Wang, B. Hong, X. Peng, X. Wang, H. Ge, J. Hu, Effects of gradient diameter on magnetic properties of FeNi alloys nanowires arrays, J. Magn. Magn. Mater. 499 (2020) 166207. https://doi.org/10.1016/j.jmmm.2019.166207.
[40] A.S. Samardak, A. V. Ognev, A.Y. Samardak, E. V. Stebliy, E.B. Modin, L.A. Chebotkevich, S. V. Komogortsev, A. Stancu, E. Panahi-Danaei, A. Fardi-Ilkhichy, F. Nasirpouri, Variation of magnetic anisotropy and temperature-dependent FORC probing of compositionally tuned Co-Ni alloy nanowires, J. Alloys Compd. 732 (2018) 683–693. https://doi.org/10.1016/j.jallcom.2017.10.258.
[41] C.I. Dobrotă, A. Stancu, Mean field model for ferromagnetic nanowire arrays based on a mechanical analogy, J. Phys. Condens. Matter. 25 (2013). https://doi.org/10.1088/0953-8984/25/3/035302.
[42] V. Vega, W.O. Rosa, J. García, T. Sánchez, J.D. Santos, F. Béron, K.R. Pirota, V.M. Prida, B. Hernando, Template-assisted copd nanowire arrays: Magnetic properties and FORC analysis, J. Nanosci. Nanotechnol. 12 (2012) 4736–4743. https://doi.org/10.1166/jnn.2012.4908.
[43] Á. Díaz-García, L.M. Moreno-Ramírez, J.Y. Law, F. Albertini, S. Frabbrici, V. Franco, Characterization of thermal hysteresis in magnetocaloric NiMnIn Heusler alloys by Temperature First Order Reversal Curves (TFORC), J. Alloys Compd. 867 (2021) 159184. https://doi.org/10.1016/j.jallcom.2021.159184.
[44] L.M. Moreno-Ramírez, V. Franco, Setting the basis for the interpretation of temperature first order reversal curve (TFORC) distributions of magnetocaloric materials, Metals (Basel). 10 (2020) 1–15. https://doi.org/10.3390/met10081039.
[45] L. Galdun, V. Vega, Z. Vargová, E.D. Barriga-Castro, C. Luna, R. Varga, V.M. Prida, Intermetallic Co 2 FeIn Heusler Alloy Nanowires for Spintronics Applications , ACS Appl. Nano Mater. 1 (2018) 7066–7074. https://doi.org/10.1021/acsanm.8b01836.

[46] B. Kunca, I. Maťko, P. Švec, I. Škorvánek, FORC Study of Magnetization Reversal and Interlayer Interactions in Rapidly Quenched Fe/Co-Based Bilayer Ribbons, Acta Phys. Pol. A. 137 (2020) 815–817. https://doi.org/10.12693/APhysPolA.137.815.
[47] H. Nath, G. Phanikumar, Martensite Transformation and Magnetic Properties of Ni-Fe-Ga Heusler Alloys, Metall. Mater. Trans. A Phys. Metall. Mater. Sci. 46A (2015) 4947–4955. https://doi.org/10.1007/s11661-015-3098-7.
[48] E. Panchenko, Y. Chumlyakov, H.J. Maier, E. Timofeeva, I. Karaman, Tension/compression asymmetry of functional properties in [001]-oriented ferromagnetic NiFeGaCo single crystals, Intermetallics. 18 (2010) 2458–2463. https://doi.org/10.1016/j.intermet.2010.09.009.
[49] R. Oshima, M. Sugiyama, F.E. Fujita, Tweed Structures Associated with Fcc-Fct Transformations in Fe-Pd Alloys, Metall. Trans. A. 19 A (1988) 803–810. https://doi.org/10.1007/bf02628361.
[50] H.R. Zhang, C. Ma, H.F. Tian, G.H. Wu, J.Q. Li, Martensitic transformation of Ni2 FeGa ferromagnetic shape-memory alloy studied via transmission electron microscopy and electron energy-loss spectroscopy, Phys. Rev. B - Condens. Matter Mater. Phys. 77 (2008) 1–12. https://doi.org/10.1103/PhysRevB.77.214106.
[51] O. Heczko, Magnetic shape memory effect and magnetization reversal, J. Magn. Magn. Mater. 290–291 (2005) 787–794. https://doi.org/10.1016/j.jmmm.2004.11.397.
[52] C.R. Pike, A.P. Roberts, M.J. Dekkers, K.L. Verosub, An investigation of multi-domain hysteresis mechanisms using FORC diagrams, Phys. Earth Planet. Inter. 126 (2001) 11–25. https://doi.org/10.1016/S0031-9201(01)00241-2.
[53] A.R. Muxworthy, A.P. Roberts, First-Order Reversal Curve (FORC) Diagrams, Encycl. Geomagn. Paleomagn. (2007) 266–272. https://doi.org/https://doi.org/10.1007/978-1-4020-4423-6_99.
[54] M.P. Proenca, C.T. Sousa, J. Escrig, J. Ventura, M. Vazquez, J.P. Araujo, Magnetic interactions and reversal mechanisms in Co nanowire and nanotube arrays, J. Appl. Phys. 113 (2013) 1–7. https://doi.org/10.1063/1.4794335.
[55] C.R.P. A. P. Roberts, D. Heslop, X. Zhao, Understanding fine magnetic particle systems through use of first-order reversal curve diagrams, Rev. Geophys. 52 (2014) 557–602. https://doi.org/10.1002/2014RG000462.
[56] M.P. Proenca, K.J. Merazzo, L.G. Vivas, D.C. Leitao, C.T. Sousa, J. Ventura, J.P. Araujo, M. Vazquez, Co nanostructures in ordered templates: Comparative FORC analysis, Nanotechnology. 24 (2013). https://doi.org/10.1088/0957-4484/24/47/475703.
[57] M.P. Proenca, J. Ventura, C.T. Sousa, M. Vazquez, J.P. Araujo, Angular first-order reversal curves: An advanced method to extract magnetization reversal mechanisms and quantify magnetostatic interactions, J. Phys. Condens. Matter. 26 (2014). https://doi.org/10.1088/0953-8984/26/11/116004.
[58] S. Shevyrtalov, H. Miki, M. Ohtsuka, A. Grunin, I. Lyatun, A. Mashirov, M. Seredina, V. Khovaylo, V. Rodionova, Martensitic transformation in polycrystalline substrate-constrained and freestanding Ni-Mn-Ga films with Ni and Ga excess, J. Alloys Compd. 741 (2018) 1098–1104. https://doi.org/10.1016/j.jallcom.2018.01.255.

Graphical abstract

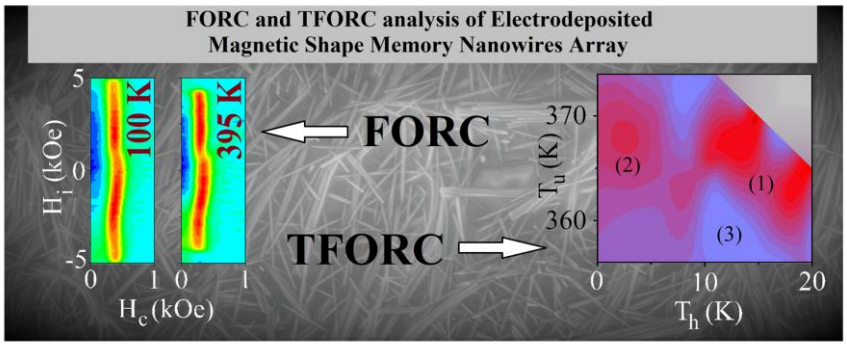


**HIGHLIGHTS**

- Classical FORC investigation of functional nanowires was performed
- Unique TFORC analysis was employed as a trivial characterization technique
- FORC and TFORC analysis showed a presence of shape memory behavior